PROCEEDINGS, Thirty-Seventh Workshop on Geothermal Reservoir Engineering
Stanford University, Stanford, California, January 30 - February 1, 2012
SGP-TR-194

MODELING AND ANALYSIS OF STIMULATION FOR FRACTURE NETWORK GENERATION

Varahanaresh Sesetty and Ahmad Ghassemi

Texas A&M University
3116 TAMU - 507 Richardson Building
College Station, TX, 77843, USA
e-mail: ahmad.ghassemi@pe.tamu.edu
varahanaresh.sesetty@pe.tamu.edu

ABSTRACT

Modeling the interaction between hydraulic fractures and pre-existing natural fractures in the formation is important to reservoir stimulation. This paper presents a boundary element-based method for modeling this interaction. The method utilizes a fully coupled fluid flow and fracture deformation. The simulation results show the hydraulic fracture trajectory, fracture aperture and pressures as a function of injection time. The fluid flow into the natural fractures and their transition to hydraulic fracture is modeled. The injection pressure profile shows the fracture complexity of the propagation process and its impact on stimulation design and proppant placement. Possible locations of secondary fracture initiation are also discussed.

INTRODUCTION

The propagation of hydraulic fracture in a naturally fractured reservoir is a subject of interest in both geothermal and unconventional petroleum reservoir development. Often, the fracturing in a reservoir having multiple natural fracture leads to a complex fracture network. In geothermal and shale reservoirs, it is believed that fracture complexity increases the heat extraction surface area, and drainage volume, respectively. However, poor placement of fracture stages can cause detrimental effects. In order to optimize the fracturing it is important to understand the HF-NF interactions and their effect on fracture system stability.

A connected fracture systems plays a major role in heat extraction from geothermal reservoirs. Hydraulic fracturing is applied to enhance the system connectivity to increase the stimulated reservoir volume. A complex fracture system that is not stable may lead to short-circuiting which decreases the life of the reservoir. Therefore it is necessary to study the generation of fracture systems and the factors that affect their evolution.

Many theoretical (Potluri, Zhu et al. 2005), experimental/analytical (Blanton 1982; Warpinski and Teufel 1987) studies have treated the interaction between natural and hydraulic fractures. However, for these analytical attempts, the in-situ stresses along the natural discontinuities were assumed not to have been affected by the hydraulic fracture, i.e., the mechanical interactions between the hydraulic fracture and the natural fractures were not considered. Numerical models have been used (Koshelev and Ghassemi, 2003; Dobroskok and Ghassemi 2004) to study the details of mechanical fracture interactions without explicit consideration of flow. Zhang et al. (2006) considered fluid flow in the hydraulic fracture and obtained the resulting pressure distribution as it intersected a single natural fracture without consideration of the details of fracture interactions. Weng et al. (2011) modeled the hydraulic fracture propagation in a formation with multiple natural fractures. But the model calculates the stress shadows separately using displacement discontinuity method to incorporate the mechanical interactions between the hydraulic fracture and the natural fractures. Pengcheng Fu et al. (2011) simulated hydraulic fracture propagation in a stochastically distributed natural fracture network. The above models do not capture the details of hydraulic fracture near natural fractures and the re-distribution of in-situ stress due to the presence of natural fracture.

In this paper, a numerical model is developed to simulate the complex fracture network while taking into account the influence of natural fractures on the in-situ stress distribution. Various cases with different fracture configurations are studied to find the evolving fracture geometry. Injection pressures and widths along the fracture are calculated and

plotted to find the possible locations for proppant screen outs and secondary fracture initiation. In this model the injection rate is allowed to change and the shear slippage is considered without further elaboration on associated induced seismicity.

NUMERICAL MODEL

Displacement discontinuity method

In this model the displacement discontinuity boundary element method is used to find fracture deformation. As this method involves dividing only the boundary into elements, it has more advantages when dealing with crack propagation problems because the amount of data handled is considerably less. In this method the fracture is divided into *n* small segments. The resultant normal and shear stresses on the fracture segments is given by (Crouch and Starfield, 1983)

$$\begin{aligned} \overset{i}{\sigma}_s &= \sum_{j=1}^{N} \overset{ij}{A}_{ss} \overset{j}{D}_s + \sum_{j=1}^{N} \overset{ij}{A}_{sn} \overset{j}{D}_n \\ \overset{i}{\sigma}_n &= \sum_{j=1}^{N} \overset{ij}{A}_{ns} \overset{j}{D}_s + \sum_{j=1}^{N} \overset{ij}{A}_{nn} \overset{j}{D}_n \end{aligned} \quad \text{(i=1 to N)} \quad (1)$$

Where $\overset{ij}{A}_{ss}, \overset{ij}{A}_{sn}, \overset{ij}{A}_{ns} \text{ and } \overset{ij}{A}_{nn}$ are the boundary influence coefficients for the stresses. The above system of linear equations is solved for elemental displacement discontinuities of fracture segments by specifying the boundary stresses on the segments.

Joint model

The displacements along the natural fractures (joints) are solved using joint element displacement discontinuity. The joint elements have normal and shear stiffness that represents the joint surface characteristics or those of the filling material in the joint. Though the joint filling material usually deforms non-linearly, for simplicity a linear deforming element is used in this problem as shown in Fig 1.

Given the far field stresses $\left(\sigma_{ij}\right)_0^{\infty}$ and stresses acting on the joint element, the total joint deformation i.e. sum of initial (displacements due to initial stresses on the joint) and induced (displacements due to induced stresses caused disturbance created by fracturing in the formation) can be calculated from the following set of linear equations:

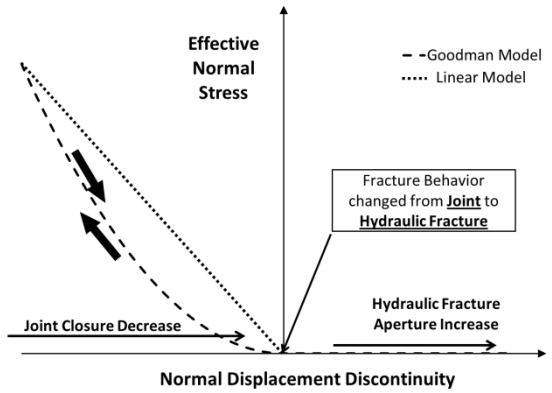

Fig 1: Goodman Joint model and a linear joint model. In Goodman model the closure reaches an asymptotic value at high values of normal stress.

$$\begin{aligned} -\left(\overset{i}{\sigma}_s\right)_0^{\infty} &= \sum_{j=1}^{N} (\overset{ij}{A}_{ss} \overset{j}{X}_s + \overset{ij}{A}_{sn} \overset{j}{X}_n) \\ -\left(\overset{i}{\sigma}_n\right)_0^{\infty} &= \sum_{j=1}^{N} (\overset{ij}{A}_{ns} \overset{j}{X}_s + \overset{ij}{A}_{nn} \overset{j}{X}_n) \end{aligned} \quad (2)$$

$(1 \le i \le M)$

$$\begin{aligned} -\left(\overset{i}{\sigma}_s\right)_0^{\infty} &= \overset{i}{K}_s \overset{i}{X}_s + \sum_{j=1}^{N} (\overset{ij}{A}_{ss} \overset{j}{X}_s + \overset{ij}{A}_{sn} \overset{j}{X}_n) \\ -\left(\overset{i}{\sigma}_n\right)_0^{\infty} &= \overset{i}{K}_n \overset{i}{X}_n + \sum_{j=1}^{N} (\overset{ij}{A}_{ns} \overset{j}{X}_s + \overset{ij}{A}_{nn} \overset{j}{X}_n) \end{aligned} \quad (3)$$

$(M+1 \le i \le N)$

Where N is the total number of elements and M is the number of normal elements. The K_s, K_n are shear and normal stiffness's of a joint element and X_s, X_n are the total joint shear and normal deformations respectively. The maximum deformation of a joint element is limited by its closure value (see Fig 1). For a joint in equilibrium condition (i.e., joint do not deform due to initial stresses) the far field stresses are zero in the above equation. Refer to Table 1 for complete joint properties used in this model.

Fluid flow

The governing equations for fluid flow in the fracture are continuity equation i.e.:

$$\frac{\partial q}{\partial x} + \frac{\partial A}{\partial t} + ql = 0 \quad (4)$$

Where A is the cross-sectional area of the fracture and q_l is the fluid leakoff rate (volume rate of fluid leakoff into the formation per unit length of fracture

with units m^2/s), that is assumed to be zero in this model.

And the simplified Navier-Stokes equation for viscous flow through smooth parallel plates is (also called lubrication equation):

$$q = -\frac{w^3}{12\mu}\frac{\partial p}{\partial x} \qquad (5)$$

For fluid flow, the initial and boundary conditions used are:

$$w(x,0) = 0$$

At injection point

$q(0,t) = q_0$ (Here q is injection volume rate per unit meter of fracture height)

and at fracture tip

$$p(L,t) = P_{tip}$$

In this model the net pressure (σ_h-p) at the fracture tip is assumed to be zero, for fracture propagation.

Connected fracture system

The flow through a connected fracture system is solved by applying the continuity condition at the fracture intersection points. For example if there are *n* fracture segments (see Fig 2) connected at intersection *i*, the resultant fluid inflow or outflow q_i (from *i*) is given as:

$$\sum_{j=1}^{n} \frac{(w_{ij})^3}{12\mu}\frac{p_i - p_j}{L_{ij}} = q_i \qquad (6)$$

Where p_i and p_j are the pressures in their respective segments, w_{ij} and L_{ij} are the width and length between the fracture segments *i* and *j*.

FLUID FLOW AND FRACTURE DEFORMATION COUPLING

Displacement discontinuity method is used to find the fracture deformation for a given pressure distribution. The fluid injection into the fracture results in change in fluid pressure inside the fracture, which in turn changes the fracture aperture. Thus, the fracture pressure and aperture depend on each other. To solve this problem the fluid flow is coupled iteratively with DD in order to obtain a unique solution. The coupling is done by assuming the initial pressure distribution in the fracture to find initial DD. The DD calculated is used in the flow solver to find the fluid pressure. This modified fluid pressure is substituted in DD and the same process is continued till a unique solution is obtained.

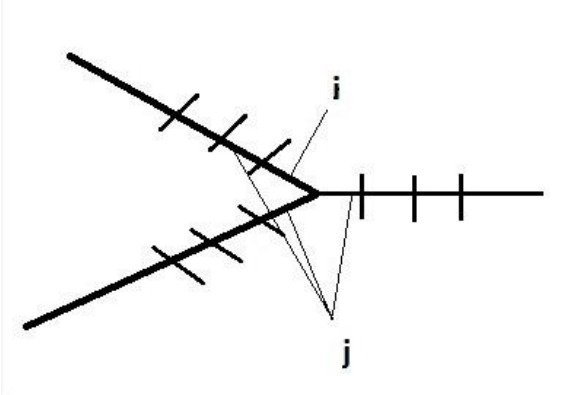

Fig 2: A basic connected fracture system showing intersection i and connected elements j.

FRACTURE PROPAGATION

The fracture tips are allowed to propagate after every time step without checking the condition for propagation. The structural criterion (Dobroskok et al. 2005) is used to track the fracture path during its propagation. For more accurate results a special fracture tip element (Yan et al. 2004) is used to find the tensile and shear stresses ahead of the fracture tip. The fracture is allowed to propagate in the tensile (Mode I) and shear (Mode II) modes depending on the tensile and shear stresses ahead of its tip. The fractures coalescence is allowed when the distance between the approaching fracture tip and the natural fracture is less than the size of an approaching fracture tip element. Currently, the conditions for fracture crossing, arrest, offset and mechanics involved in fracture coalescence are ignored.

NUMERICAL RESULTS

Case 1: Hydraulic fracture approaching natural fracture that is in equilibrium with the far-field stress.

In this case the geometrical configuration of hydraulic fracture and natural fracture shown in Fig. 3 is considered. Since the natural fracture is assumed to be in equilibrium state, it does not deform under initial stress field, also the hydraulic aperture is assumed as zero in this case. The injection rate, viscosity of the fluid and insitu-stresses along with all other parameters are listed in Table 1. Fluid is injected at the center of hydraulic fracture and the hydraulic fracture tip facing the natural fracture is allowed to propagate. For the configuration shown, the hydraulic fracture intersects the natural fracture at a right angle.

Table 1: Input parameters for all cases.

Parameter	Value	Units
Injection rate (q_0)	0.001	m^2/s
Fluid viscosity (μ)	0.001	Kg/m.s
Young's modulus (E)	27	GPa
Poisson's ratio (ν)	0.25	
(σ_H), (σ_h)	5, 4	MPa
Normal joint stiffness (K_n)	5	GPa/m
Shear Joint stiffness joint (K_s)	2.5	GPa/m
Hydraulic aperture (case 2)	0.1	mm
Maximum joint closure (δ_m)	0.3	mm

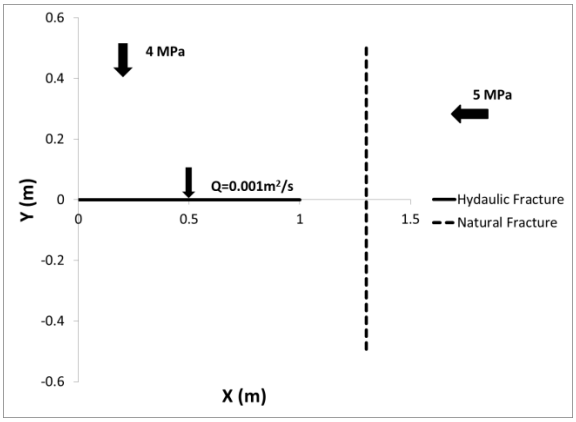

Fig 3: geometrical configuration of hydraulic fracture and natural fracture in case 1.

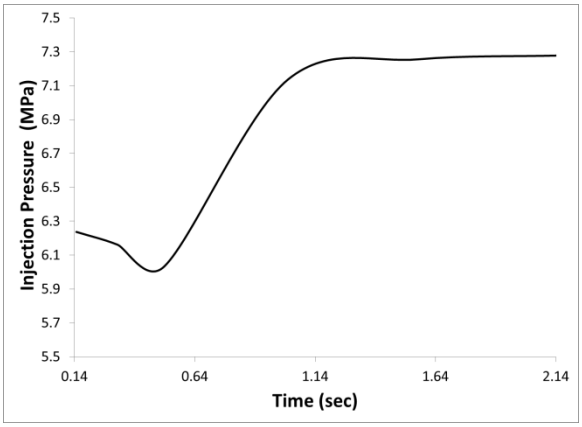

Fig 4: Variation of fluid pressure at injection point with time.

Because the energy needed to keep the propagation of the hydraulic fracture decreases once it is initiated, the pressure at the injection point is observed to be decreasing until the hydraulic fracture (HF) tip arrives at the natural fracture (Fig 4). A sudden increase in the injection pressure is observed when the hydraulic fracture intersects the natural fracture (NF). This can be attributed to the higher pressures needed to open the natural fracture because of the closure stress acting on the natural fracture. After intersection, the injection pressure reaches a constant value as time elapses to maintain the fracture network width, compensating for the pressure losses along the natural fracture and at the HF bends. The of increase in injection pressure when the HF intersects the NF depends on many factors such as the distance between the hydraulic fracture and natural fracture, geometrical configuration, closure stress, fluid properties. Some of these effects will be studied in the later sections.

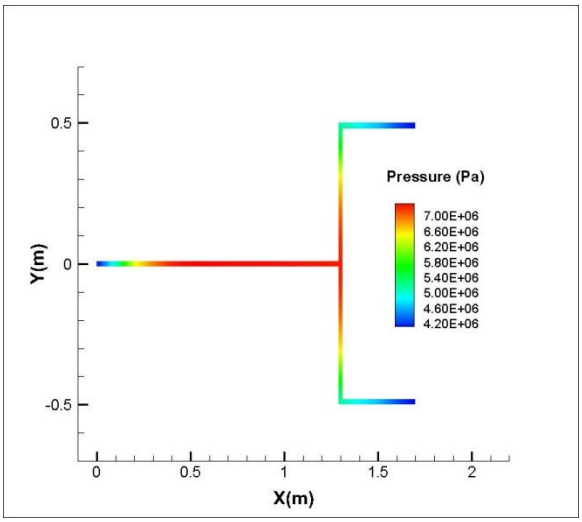

Fig 5: Contour plot of fluid pressure in the fracture network at 1.74 sec. A large increase in pressure at intersection is evident.

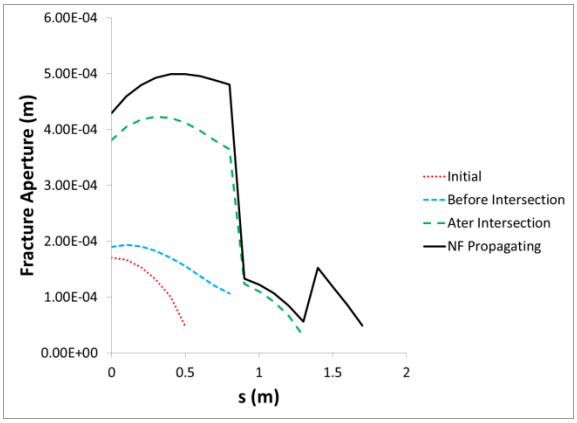

Fig 6: Width profile along the hydraulic and natural fracture at various instants.(S ranging from 0-0.8 m, 0.8-1.3m, and 1.3-1.7 m correspond to the HF, pre-existing natural fracture, and the propagating natural fracture, respectively)

The crack opening profiles are shown in the Fig 6 at different times of propagation. In order to make it convenient, all the crack profiles against distance

along the crack (i.e., s) from injection point are shown in a single plot.

The widths of the natural fracture are less than hydraulic fracture due to the closure stress acting on the natural fractures which need a high pressure to open it. The extended crack formed at the end of natural fracture in the direction of maximum principal stress opened more than the initial natural fracture even though the pressures are less because of the lower closure stress acting along it. This will result in constricted openings at the bends. These are the potential sites for proppant blockage and pressure losses.

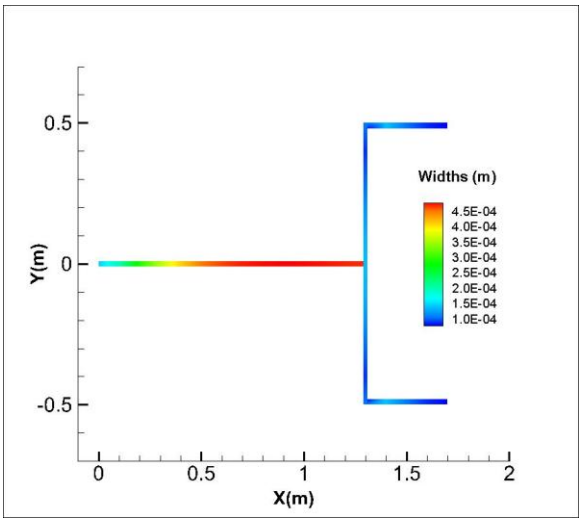

Fig 7: Contour plot of fracture width in the fracture network at time 1.74 sec. The intersection and bends act as chokes.

Case 2: HF approaching a NF which is not in equilibrium.

The geometrical configuration for this case is shown in Fig 8. The natural fracture is inclined and has a length of 4m. The fluid is injected at the inlet of the hydraulic fracture. The parameters shown in Table 1 are used for this case.

Fig 9 shows the hydraulic fracture trajectory near an inclined natural fracture. The altered in-situ stress field due to the presence of natural fracture often results in a complex fracture network. The fracture trajectory depends on the factors such as far-field stress distribution, geometry of natural fracture, hydraulic fracture and fluid properties.

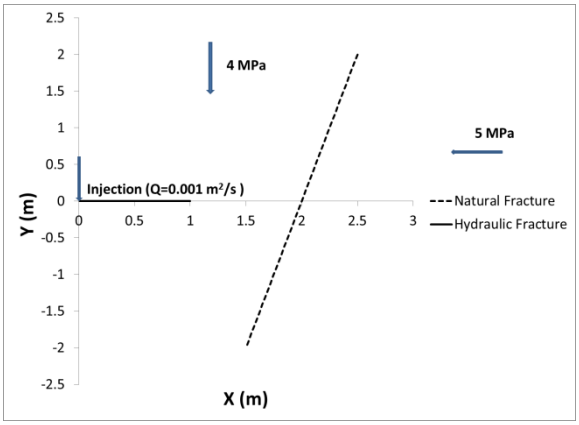

Fig 8: Geometrical configuration of hydraulic and natural fracture for case 2.

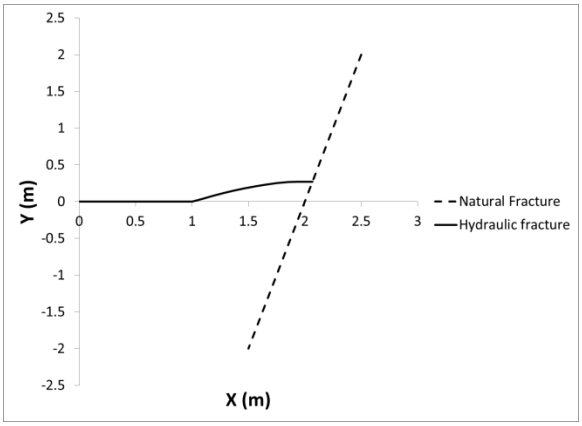

Fig 9: Simulation of hydraulic fracture trajectory for case 3. The effect of discontinuities on initial stress field and hydraulic fracture is evident from above.

As the hydraulic fracture tip reaches near the natural fracture, coalescence is applied (node to node). After the fracture coalescence, the fluid is allowed to flow into the natural fracture. To solve for the apertures along the joint, we need to distinguish between the joint elements and hydraulic fracture elements along the joint as they behave differently. To solve this problem an algorithm is implemented to calculate the apertures of natural fracture (joint). The algorithm distinguishes between contact elements (joint elements) and non-contact elements (hydraulic fracture elements) and iteratively solves for the apertures of natural fracture.

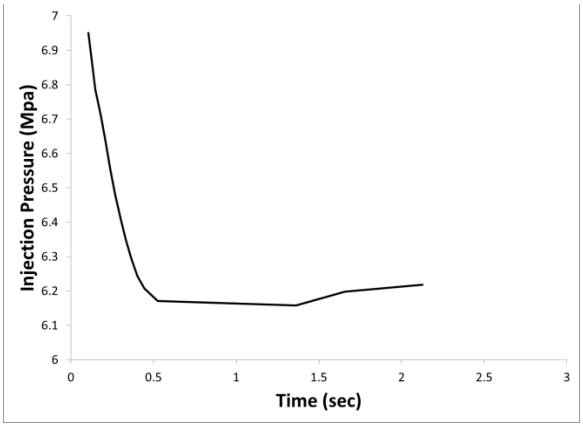

Fig 10: Variation of fluid pressure at injection point with time in case 2.

Fig 10 shows the injection pressure profile with time, the injection pressure profile follows the same trend as in case 1. The value of the injection pressure reached during intersection of hydraulic fracture and natural fracture depends on the distance between HF and NF, closure stress acting on the natural fracture and its maximum allowed closure. We can see in case 1 (Fig. 4) that the peak value of pressure is much higher compared to case 2 (Fig. 10). This can be attributed to the larger distance between the injection and intersection points (Zhang et al. 2006) in case 2. The closure value in case 2 (0.3mm, higher widths yields lower pressures along the fractures), and the low closure stress acting on the natural fracture. The injection pressure continues to increase until the entire natural fracture is jacked open.

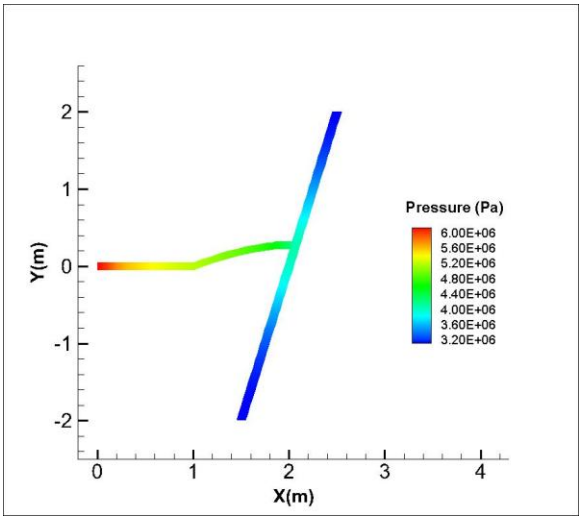

Fig 11: The contour plot of fluid pressure in case 2 fracture network at time 1.36 sec.

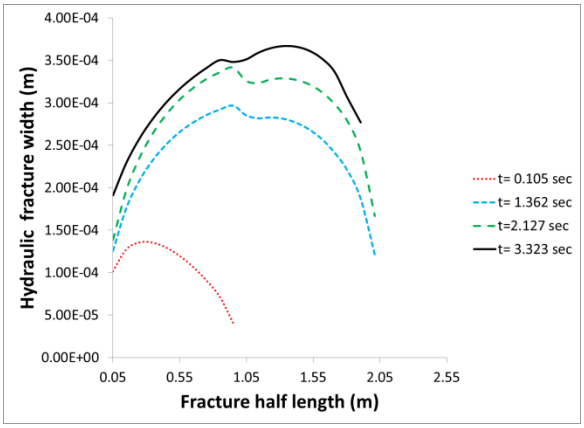

Fig 12: Hydraulic fracture opening profiles at various instants. A sudden decrease in the widths at 1 m is caused by the change in hydraulic fracture trajectory.

Fig. 12 shows the apertures of the hydraulic fracture at various times. A sharp decrease in the fracture widths at length 1m is observed and can be attributed to the change in fracture trajectory at that point. The hydraulic fracture aperture continues to increase with time as the fracture propagates but when the fracture coalescence takes place, the amount of the aperture increase is relatively higher because of the increase in pressures along the fracture after coalescence.

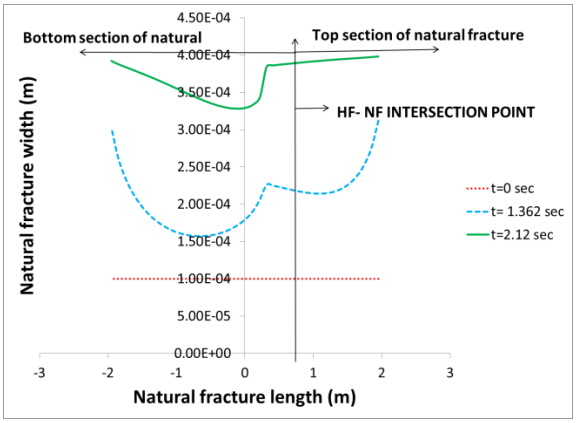

Fig 13: The natural fracture opening profiles at various instants. The widths of the top section of the NF are higher compared to its lower section because of stress shadow on that section of NF. The apertures at the end of top and bottom section of the NF are equal because the joint closure is higher at center and lower at the tip.

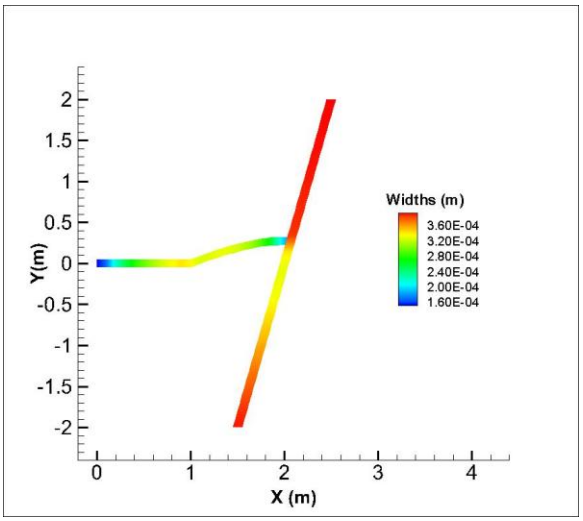

Fig 14: Contour plot of fracture width in the fracture network at 1.74 sec past injection. The kink in the HF and the lower part of NF acts as choke points.

Fig. 13 shows the apertures of natural fracture at various times. Initially, the natural fracture is assumed to be supported by pore pressure and asperities. The rough surfaces in the natural fracture account for its hydraulic conductivity. As the fluid injection continues and natural fracture is pressurized, its width will increase eventually transforming it to a hydraulic fracture. At time 1.36 sec the natural fracture has a higher width than its original hydraulic aperture. For the inclined natural fracture considered above, the top section of the natural fracture has higher widths than the bottom section. This is due to the presence of stress shadow on the lower section of the natural fracture which in this case develops by hydraulic fracture kinking. At time 2.12 sec, the entire top section of the NF is completely open while its bottom section is only partially opened. As pressure increases, this will likely result in the propagation of the top section of the natural fracture. The lower width in the bottom section of the natural fracture will act as a constriction to any proppant that might be pumped in to the natural fracture, as the fluid will continue to go in to the top section when it starts to propagate.

<u>Case 3</u>: Propagation of a hydraulic fracture in a formation with multiple natural fractures

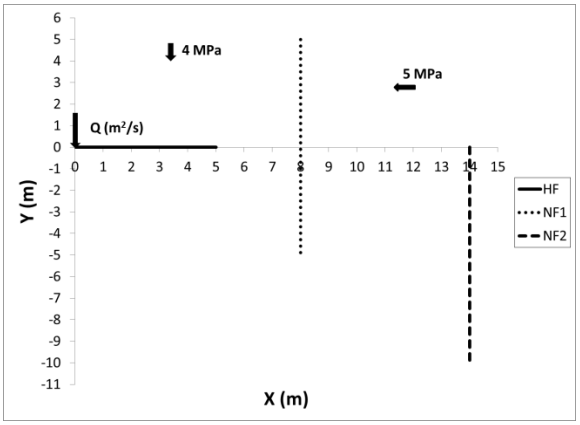

Fig 15: The geometry of hydraulic fracture and natural fractures for case 3.

Fig 15 shows the geometrical configuration of multiple natural fractures. Two parallel natural fractures each 10 m long are 6m apart are considered. The initial injection rate per unit height is 0.001 m^2/s. The fluid is injected at the left end of the hydraulic fracture. The two natural fractures are assumed to be in equilibrium condition. The fracture geometry after 35.6 sec is shown in the Figure 16. There is no fracture kinking observed in this case because the natural fractures are assumed to be in equilibrium state and all fractures are either parallel or orthogonal to the insitu stresses. As shown in Figure 16, for NF1 both tips are allowed to propagate because of its symmetry with respect to the hydraulic fracture. When the tip of NF1 intersects NF2, the fluid is allowed to flow in it and top wing of NF1 is not allowed to propagate anymore. Once the NF2 is completely open, its tips are allowed to propagate.

Fig. 17 shows the injection pressure profile for this case. The injection pressure is decreasing till it reaches the natural fracture (as the hydraulic fracture propagates, the aperture increases which results in low pressure losses).

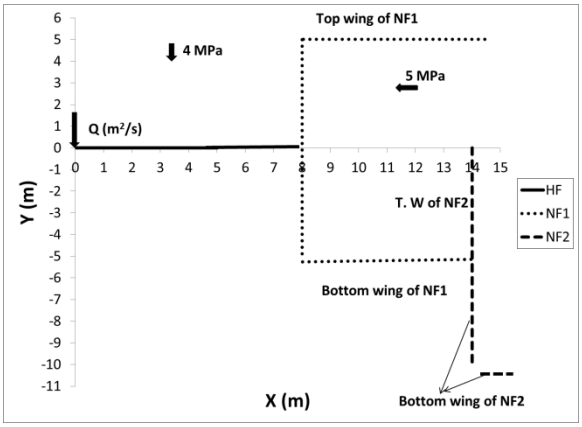

Fig 16: The geometry of hydraulic fracture and natural fractures for case 3 after 35 sec.

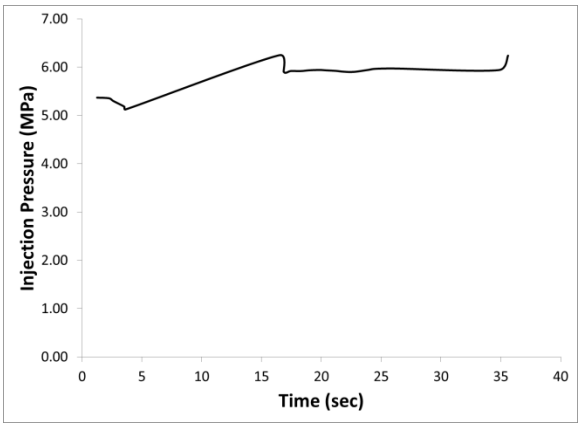

Fig 17: Injection pressure profile with time. There is a steep increase in injection pressure when the HF intersects NF1. Then pressure decreases when NF1 starts to propagate and again increase when NF2 propagates as the network become more complex.

At the point of intersection there is surge in pressure similar to the previous cases, because the natural fracture has to open against high in-situ stress. We can see that the injection pressure has decreased once the natural fracture (NF1) started to propagate and it is nearly constant as the natural fracture (NF1) propagates. The increase is to compensate for pressure losses at the bend of NF1 (less aperture in NF1 leads to high pressure losses also). Here we can observe that there is no steep increase in injection pressure after the lower tip of NF1 intersects NF2 (unlike after HF intersection with NF1). This is because the high injection pressure that is maintained while propagating NF1 is sufficient to open NF2 but, the pressure continues to increases even when NF2 propagates because the fracture network has become more complex with interaction between NF1 and NF2. Thus, a high injection pressure is needed in order to keep entire fracture network open.

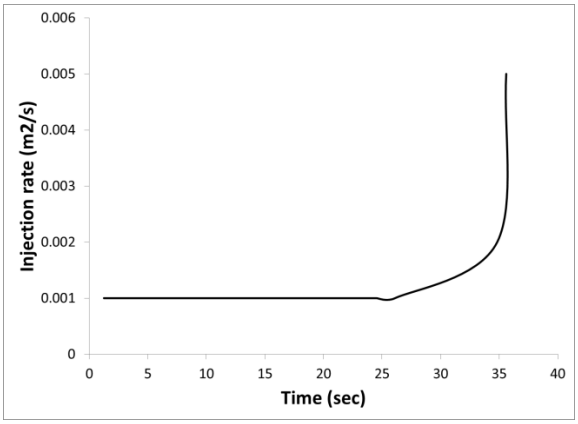

Fig 18: The injection rate vs. with time. The injection rate starts to increase when the fracture network becomes more complex.

Figure 18 shows the injection rate profile. The initial injection rate is $0.001 m^2/s$ and is maintained until the tip of NF1 intersects NF2. The high injection rate is needed when the fracture network has become complex as higher energy is needed to keep the entire fracture network open.

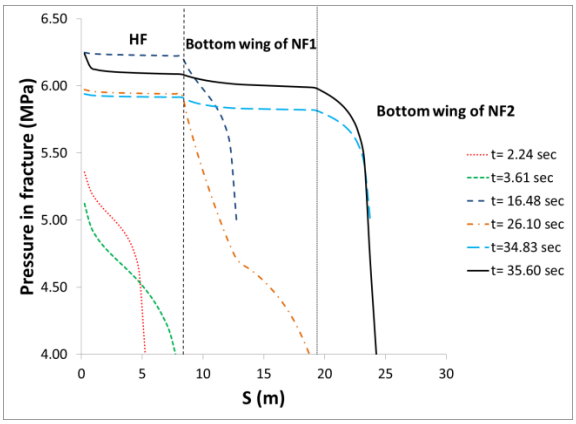

Fig 19: The pressure profile along the HF and the bottom wings of NF1 and NF2. There is a large increase in pressure along the fractures when HF intersects NF1. When NF1 intersects NF2, the pressure at intersection of NF1 and NF2 increases but there is no significant change in pressure along the HF.

Figure 19 shows the pressure profile along the hydraulic fracture (s=0-8m) and bottom wings of NF1 and NF2. The hydraulic fracture intersects NF1 at s=8m and the bottom wing tip of NF1 intersects NF2 at s=19m. It can be observed that when the HF intersects NF1 the pressure along the fracture increases (t= 16.48 sec). At t= 34.83 sec the bottom wing tip of NF1 intersected NF2 resulting in high pressure at their intersection s=19m (compare with pressures along the fracture at time 26.10 sec), but there is no pressure rise along the hydraulic fracture(s=0-8m). The pressure continues to increase as NF2 propagates. Similarly, Fig 20 shows the pressure along the hydraulic fracture and top wings of NF1 and NF2. There it can be observed that at time 34.83 sec the pressure along the top wing of NF1 is less than bottom wing of NF2 because once the bottom wing tip of NF1 intersected NF2 the top wing of NF1 is stopped to propagate. Whereas along the top wing of NF2 we can see much less pressure because of the interaction between of NF1 and top wing of NF2; the fluid tries to enter into the least resistance path that is bottom wing of NF2. As fluid injection is continued, there is an increase in pressure along the top wing of NF2 at time 35.6 sec.

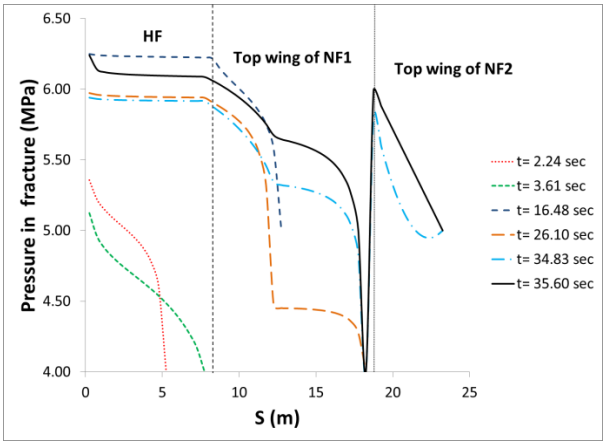

Fig 20: The pressure profile along the HF and top wings of NF1 and NF2. The pressure in top wing of the NF1 is less than the bottom wing of NF2. This is because of the interaction between NF1 and NF2.

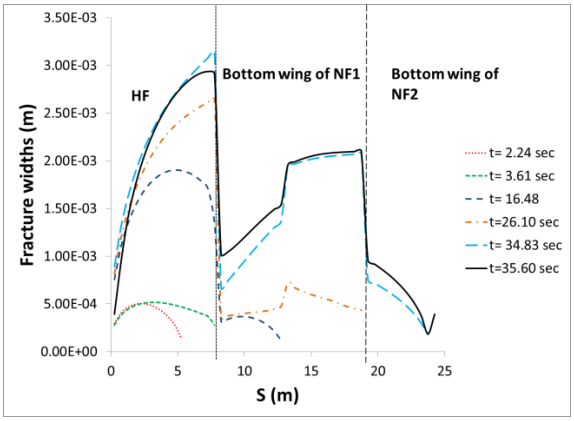

Fig 21: shows the profile of fracture widths of bottom wings of HF, NF1 and NF2 corresponding to the pressures shown in fig 19

Fig 21 shows the width profile along the hydraulic fracture and bottom wings of NF1 and NF2. The jump in widths at s= 8m, 13m and 19m are caused by the stress anisotropy along the fractures. Fig 22 shows width profile along the hydraulic fracture and top wing of NF1 and NF2. The widths of top wing of NF1(s=8-13m) are less than the widths of bottom wing of NF2(s=8-13m) at t= 26.10 sec because the bottom wing of NF2 opened easily with the influence of NF2. The widths of bottom wing of NF1 (s=13-19m) are more than top wing of NF1 (s=13-19m) because of the high-pressure build up behind the tip of the bottom wing of NF1 due to the resistance from opening of NF2 leads to high widths in that section even before the intersection of NF1 and NF2 (t=26.1 sec). At t= 34.83 sec, the tip of NF1 intersected NF2, which lead to high pressures along the bottom wing of NF1, giving it more widths than top wing of NF1. Fig 22 shows the top wing of NF1 is not open even at 35.60 sec because of huge stress concentration between NF1 and NF2. As a result, the top wing of NF2 will not propagate since it was not opened.

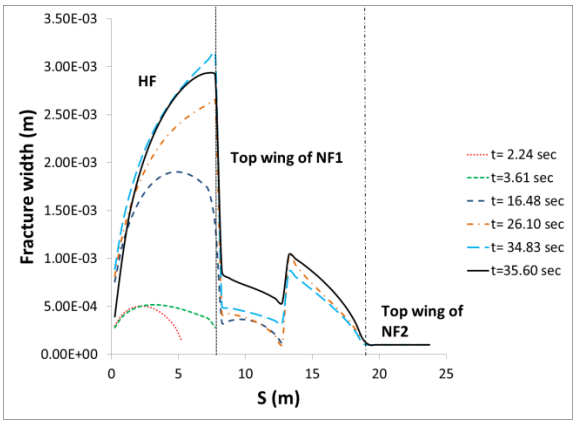

Fig 22: The profile of fracture widths of top wings of HF, NF1 and NF2 corresponding to the pressures shown in Fig 20.

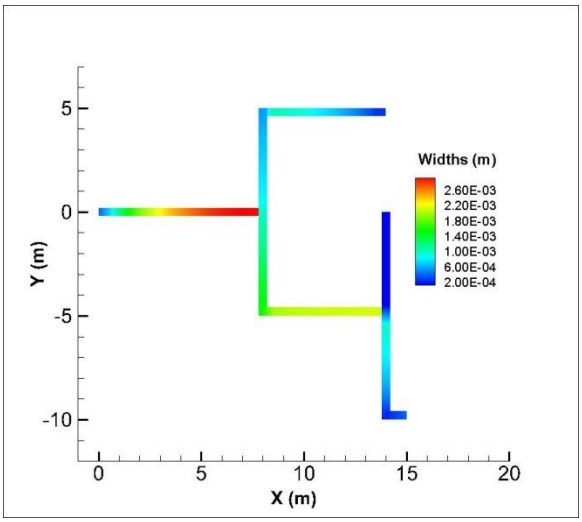

Fig 23: contour plot of fracture widths at 35 sec. The top wing of NF2 completely remained unopened due to the influence of NF1.

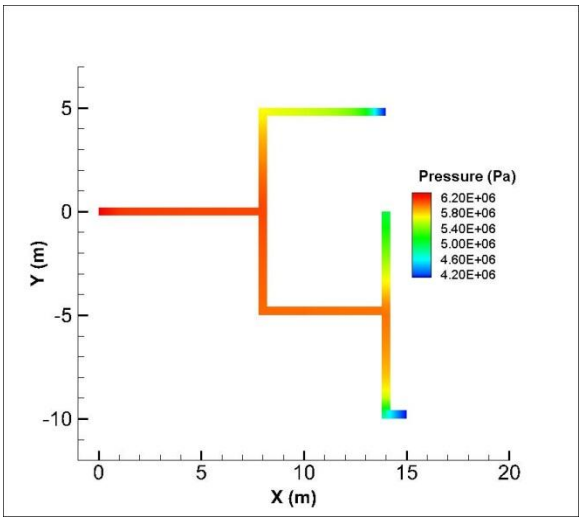

Fig 24: contour plot of fracture pressures at 35 sec. The large increase in bottom wings of NF1 and NF2 are evident. Secondary fractures may initiate from this fracture network due to its instability (see Fig 18).

CONCLUSIONS

The effect of pre-existing natural fracture in both equilibrium and a non-equilibrium state on hydraulic fracture is studied. Pre-existing fracture in non-equilibrium state leads to a more complex hydraulic fracture geometry. The sites of facture kinking, intersections, and bends act as chokes and can cause proppant blockages. The injection pressure tends to decrease until the hydraulic fracture intersects natural fracture. The injection pressure will increase during the opening of natural fracture until it propagates. The amount of increase in injection pressure during intersection depends on factors such as injection rate, distance between injection point and intersection point, joint closure value, and closure stress acting on the joint. When the tip of NF1 intersected NF2 there is an increase in the pressure at the intersection of NF1 and NF2 but, there is no significant pressure raise at the injection point. This indicates that the injection pressure profile may not be very useful for detecting fracture intersection events. The injection rate increases with the fracture complexity to provide the necessary energy to keep the fracture network open. The injection rate profile reflects the complexity of the fracture network. As the fracture network becomes more complex, the injection pressure and injection rate increases significantly. This can lead to creating new secondary fractures at the weak sections of the fracture network.

REFERENCES

Batchelor, G.K. (1967), "Arn Introduction to Fluid Dynamics," Cambridge, UK: Cambridge University Press, Original edition, ISBN 0521 663962.

Blanton, T.L. (1982), "An Experimental Study of Interaction Between Hydraulically Induced and Pre-Existing Fractures," *SPE Unconventional Gas Recovery Symposium*, Pittsburgh, Pennsylvania, SPE of AIME.

Cooke, M.L. and Underwood, C.A. (2001), "Fracture Termination and step-over at Bedding Interfaces due to Frictional slip and Interface opening," *Journal of Structural Geology* **23,** 223-238.

Crouch, S.L. and Starfield, A.M. (1983), "Boundary Element Methods in Solid Mechanics," London: George Allen & Unwin.

Dobroskok, A. and Ghassemi, A. (2004), "Crack Propagation, Coalescence and Re-initiation in Naturally Fractured Rocks,". *In GRC Trans*, **28**, 285-288.

Dobroskok, A., Ghassemi, A. and Linkov, A. (2005), " Extended Structural Criterion for Numerical Simulation of Crack Propagation and Coalescence under Compressive Loads," *International Journal of Fracture*, **133**, 223-246.

Fu, P., Johnson, S.M., Hao, Y. and Carrigan, C. R. (2011), "Fully Coupled Geomechanics and Discrete Flow Network Modeling of Hydraulic Fracturing for Geothermal Applications," *Thirty-Sixth Workshop on Geothermal Reservoir Engineering*, Stanford University, Stanford, California, January 31 - February 2.

Koshelev, V. and Ghassemi, A. (2003), "Numerical Modeling of Stress Distribution and Crack Trajectory near a Fault or a Natural Fracture," *Soil-Rock America Symp*. Boston.

Koshelev, V. and Ghassemi, A. (2003), "Hydraulic Fracture Propagation near a Natural Discontinuity," *Twenty-Eight Workshop on Geothermal Reservoir Engineering, Stanford University*, Stanford, California.

Nordgren, R.P. (1972), "Propagation of a Vertical Hydraulic Fracture," *Society of Petroleum Engineers Journal*, 12, 306-314.

Potluri, N.K., Zhu, D. (2005), "The Effect of Natural Fractures on Hydraulic Fracture Propagation," *SPE European Formation Damage Conference*, Sheveningen, The Netherlands, SPE.

Renshaw, C.E. and Pollard, D.D (1995), "An Experimentally Verified Criterion for Propagation across Unbounded Frictional Interfaces in Brittle, Linear Elastic Materials," *International Journal of Rock Mechanics and*

Mining Science & Geomechanics Abstracts, **32**(3), 237-249.

Thiercelin, M.J. and Makkhyu, E. (2007), "Stress Field in the Vicinity of a Natural Fault Activated by the Propagation of an Induced Hydraulic Fracture," *Taylor & Francis Group*, London**,** 1617-1624.

Weng, X., Kresse, O., Cohen, C., Wu, R. and Gu, H., Schlumberger (2011), "Modeling of Hydraulic Fracture Network Propagation in a Naturally Fractured Formation," SPE 140253, *SPE Hydraulic Fracturing Technology Conference and Exhibition*, Woodlands, Texas, USA, 24–26 January.

Warpinski, N.R. and Teufel, L.W. (1987). "Influence of Geologic Discontinuities on Hydraulic Fracture Propagation," (includes associated papers 17011 and 17074) *SPE Journal of Petroleum Technology* **39**(2), 209-220.

Warpinski, N.R. and Wolhart, S.L. (2004), "Analysis and Prediction of Microseismicity Induced by Hydraulic Fracturin," *SPE Journal* **9**(1), 24-33.

Wu, H. and Chudnovsky, A. (2004), "A Map Of Fracture Behavior In The Vicinity Of An Interface," *Gulf Rocks 2004, the 6th North America Rock Mechanics Symposium (NARMS)*, Houston, Texas, ARMA.

Xing, Z. and David, J.S. (2002), "Numerical Modelling and Analysis of Fluid Flow and Deformation of Fractured Rock Masses", Elsevier Science Ltd, UK

Yan, X. (2004), " A Special Crack Tip Displacement Discontinuity Element," *Mechanics Research Communications*, **31**(6), 651-659.

Zhang, X. and Jeffrey R.G. (2006), "The Role of Friction and Secondary Flaws on Deflection and Re-initiation of Hydraulic Fractures at Orthogonal Pre-Existing Fractures," *Geophysical Journal International*, **166**, 1454-1465.